4 Dark Matter Detection with XENON and DARWIN

Peter Barrow, Laura Baudis, Yanina Biondi, Adam Brown, Chiara Capelli, Michelle Galloway, Andreas James, Shingo Kazama, Gaudenz Kessler, Alexander Kish, Chris Marentini, Daniel Mayani, Francesco Piastra, Yuehuan Wei, Julien Wulf

in collaboration with: Albert Einstein Center for Fundamental Physics Bern, Columbia University, UCLA, UCSD, INFN, University of Münster, Coimbra University, Subatech, The Weizmann Institute of Science, University of Mainz, SJTU, MPIK Heidelberg, Stockholm University, Rice University, University of Chicago, University of Bologna, Nikhef and Amsterdam University, Purdue University, NYU of Abu Dhabi

(XENON Collaboration)

Astronomical and cosmological observations reveal that the vast majority of the matter and energy content of our universe is invisible – or dark – and interacts neither strongly nor electromagnetically with ordinary matter. Results from the Planck satellite [1] show that about 68% of the overall budget is dark energy, leading to the observed accelerated expansion of the cosmos. Another 27% is composed of dark matter, a yet-undetected form of matter whose presence is needed to explain the observed large-scale structures and galaxies. While dark matter interacts gravitationally with baryonic matter, any additional interactions, if existing, must be very weak with extremely small cross sections [2]. Because the Standard Model of particle physics does not accommodate dark matter, the observationally-driven need for its existence is one of the strongest indications for physics beyond the standard model. The direct detection and subsequent characterisation of dark matter particles is, therefore, one of the major experimental challenges of modern particle and astroparticle physics [3,4]. Many theories beyond the Standard Model predict viable candidates; one particular class are Weakly Interacting Massive Particles (WIMPs) [3,5].

One concept to detect dark matter is based on dual-phase noble gas time projection chambers (TPCs), where the prompt scintillation light (S1) and the delayed proportional scintillation light signal from the charge (S2) are measured. Both signals are employed for a precise reconstruction of the event vertex and to suppress backgrounds by rejection of multiple-scatter interactions, as dark matter particles are expected to interact only once. The charge-to-light ratio S1/S2 is exploited to separate the expected signal, namely nuclear recoils (NR), from the dominant electronic recoil (ER) background.

The XENON100 experiment [6, 7], a liquid xenon (LXe) TPC with a 62 kg active target, has reached its sensitivity goal and excluded spin-independent WIMP-nucleon cross sections above $1 \times 10^{-45}\,\mathrm{cm}^2$ at a WIMP mass of $55\,\mathrm{GeV}/c^2$ [8]. These constraints are superseded by the results from the LUX [9] and PANDAX [10] collaborations. While LUX operated a 250 kg TPC at SURF, PANDAX operates a 500 kg detector at the JinPing laboratory. They exclude spin-independent WIMP-nucleon scattering cross sections above $1.1 \times 10^{-46}\,\mathrm{cm}^2$ at $50\,\mathrm{GeV}/c^2$.

The next increase in sensitivity will come from XENON1T, which operates a total of 3.2 t of liquid xenon inside a cryostat surrounded by a large water Cherenkov shield. We successfully commissioned the XENON1T detector at the Laboratori Nazionali del Gran Sasso (LNGS) and started the first science run in November 2016. In the following, we will present our latest XENON100 results and the status of the XENON1T experiment. We will then describe the progress on the next-generation of dark matter detectors XENONNT and DARWIN and conclude with current R&D activities of our group.

[1] P. A. R. Ade *et al.* [Planck Collaboration], Astron. Astrophys. **571** (2014) A16.

[2] M. W. Goodman and E. Witten, Phys. Rev. D **31** (1985) 3059.

[3] G. Bertone, D. Hooper and J. Silk, Phys. Rept. **405** (2005) 279.

[4] L. Baudis, Phys. Rev. G **43** (2016) no.4, 044001.

[5] G. Jungman, M. Kamionkowski and K. Griest, Phys. Rept. **267** (1996) 195.

[6] E. Aprile *et al.* [XENON Collaboration], Phys. Rev. Lett. **107** (2011) 131302.

[7] E. Aprile *et al.* [XENON Collaboration], Astropart. Phys. **35** (2012) 573.

[8] E. Aprile *et al.* [XENON Collaboration], Phys. Rev. D **94** (2016) no.12, 122001.

[9] D. S. Akerib *et al.* [LUX Collaboration], Phys. Rev. Lett. **118** (2017) no.2, 021303.

[10] C. Fu *et al.* [PandaX Collaboration], Phys. Rev. Lett. **118** (2017) no.7, 071301.

4.1 Inelastic WIMP-nucleus interaction and search of bosonic super-WIMPs with XENON100

XENON100 is a 161 kg double-phase xenon TPC, which employs two arrays of low-radioactivity, VUV-sensitive photomultipliers (PMTs) to detect the prompt (S1) and charge-induced proportional (S2) scintillation light signals induced by particles interacting in the target volume, containing 62 kg of ultra-pure liquid xenon (LXe). The remaining 99 kg of LXe act as an active veto shield against background radiation. The XENON100 detector concluded acquisition of science data in 2016 and we are completing analyses for several physics channels. In the end of 2016, after a combined run analysis and an integrated period of 477 live days, the experiment has reached a sensitivity of 1.1×10^{-45} cm^2 at 50 GeV/c^2 and 90% confidence level on the spin-independent elastic WIMP-nucleon scattering cross section [11].

Apart from the standard WIMP analyses, at UZH we have focussed on the study of inelastic WIMP-nucleus interactions and on a search for bosonic super-WIMPs. Both manuscripts are under review by the collaboration. The first study is on the spin-dependent, inelastic scattering of WIMPs on nuclei, which induces a transition of ^{129}Xe to a low-lying excited nuclear state (the $3/2^+$ state, 39.6 keV above the $1/2^+$ ground state) [12]. The experimental signature is a NR detected simultaneously with the prompt de-excitation photon [13]. The region of interest (ROI) is based on ^{241}AmBe calibration data, as shown in Fig. 4.1, left, and extends from 60 pe to 210 pe for the prompt, and from 4×10^3 pe to 16×10^3 pe for the proportional scintillation, respectively. The ROI is divided into nine sub-regions, which contain a similar number of expected background events. The control regions are used for cross-checks of the background shape distribution and are selected to be as close as possible to the ROI. The distribution of events in the ROI is shown in Fig. 4.1, centre: a total of 764 events are observed, with an expected background of 756 $\pm$5 (stat) $\pm$55 (sys) events. This result is interpreted via a binned profile likelihood approach, and a 90% CL$_s$ confidence level limit [14] is set on the spin-dependent WIMP-nucleon cross section as a function of the WIMP mass (shown in Fig. 4.1, right). With a minimum of 3.3×10^{-38} cm^2 at 100 GeV/c^2, it is the most stringent result in this interaction channel.

At UZH we also searched for bosonic super-WIMPs [15], which are warm dark matter candidates with masses at the keV-scale that could couple electromagnetically to Standard Model particles via the axio-electric effect. The expected signature is a mono-energetic peak at the super-WIMP's rest mass. Compared to an analogous search for axion-like particles in [16], we extended the mass range to 125 keV and employed both scintillation and ionisation signals to determine the energy scale, thus improving the energy resolution from 14%, based on S1-only, to 5.7% at 100 keV. The distribution of events in the ROI is shown in Fig. 4.2, left, together with the expected signal for different pseudo-scalar bosonic super-WIMP masses, an axio-electric coupling $g_{Aee} = 5\times10^{-12}$, and a local density of 0.3 GeV/cm^3. The profile likelihood analysis showed that our data is compatible with the background model. We set competitive limits in the 8-50 keV/c^2 mass range (see Fig. 4.2, centre and right), excluding couplings to electrons $g_{Aee} > 3\times10^{-13}$ and $\alpha/\alpha' > 2\times10^{-28}$ at 90% C.L. for pseudo-scalar and vector super-WIMPs.

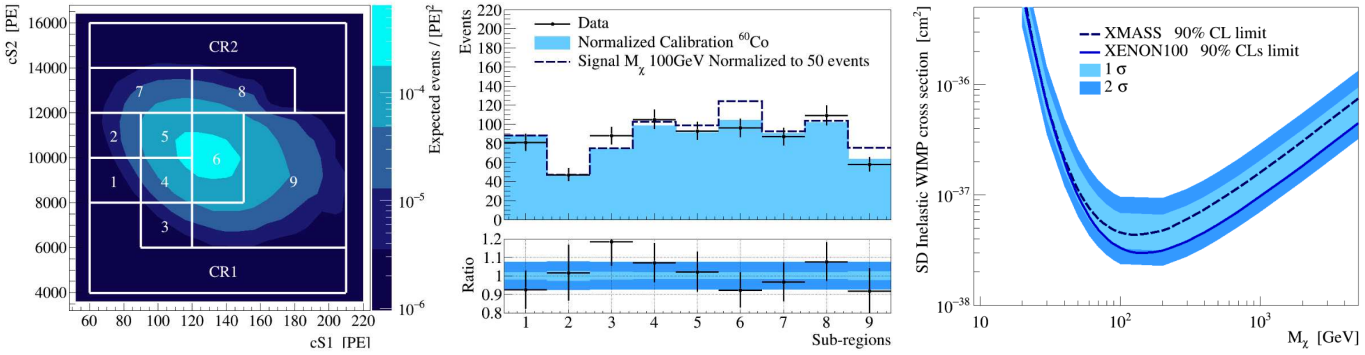

FIG. 4.1 – (Left): Signal distribution for inelastic WIMP-^{129}Xe interactions obtained from a Monte Carlo simulation of a 100 GeV/c^2 WIMP, normalised to 50 events. The signal (1-9) and control (CR1, CR2) regions are indicated. (Centre): Distribution of observed events in the region of interest (data points), along with the normalised distribution from calibration data (filled histogram), and expected signal (blue dashed). The bottom panel displays the ratio between data and expected background, where the light and dark blue shaded areas represent the statistical and systematic uncertainties on the background expectation, respectively. (Right): Upper limit (blue curve) on the WIMP-nucleon cross section in a function of the WIMP mass, together with result from the XMASS experiment (dashed) [17].

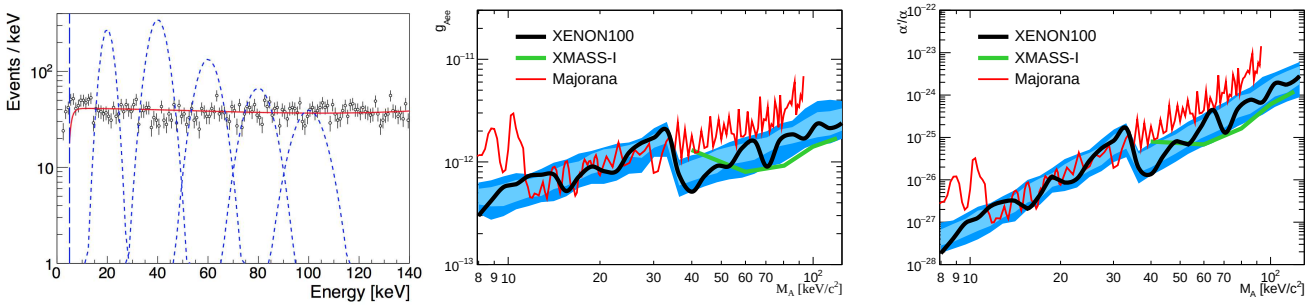

FIG. 4.2 – (Left): Distribution of events (data points) in the super-WIMP search region, between 5 and 140 keV. Also shown is the background model (red curve) along with the expected signal for super-WIMPs with various pseudo-scalar masses, and an axio-electric coupling $g_{Aee} = 5\times10^{-12}$ (blue dashed peaks). (Centre and right): The 90% C.L. upper limits on the coupling of the pseudo-scalar and vector super-WIMPs, respectively, in a function of particle mass, together with the results from XMASS-I [18] and Majorana [19].

[11] E. Aprile *et al.* [XENON Collaboration], Phys. Rev. D **94** (2016) no.12, 122001.

[12] J. R. Ellis, R. A. Flores and J. D. Lewin, Phys. Lett. B **212** (1988) 375.

[13] L. Baudis, G. Kessler, P. Klos, R. F. Lang, J. Menèndez, S. Reichard and A. Schwenk, Phys. Rev. D **88** (2013) no.11, 115014.

[14] A. L. Read, In *Geneva 2000, Confidence limits* 81-101.

[15] M. Pospelov, A. Ritz and M. B. Voloshin, Phys. Rev. D **78** (2008) 115012.

[16] E. Aprile *et al.* [XENON Collaboration], Phys. Rev. D **90** (2014) no.6, 062009, Erratum: [Phys. Rev. D **95** (2017) no.2, 029904].

[17] H. Uchida *et al.* [XMASS-I Collaboration], PTEP **2014** (2014) no.6, 063C01.

[18] K. Abe *et al.* [XMASS Collaboration], Phys. Rev. Lett. **113** (2014) 121301.

[19] N. Abgrall *et al.* [Majorana Collaboration], arXiv:1612.00886 [nucl-ex].

4.2 The first science run with XENON1T

The design of the XENON1T experiment started in 2010, while the underground construction work in LNGS Hall B started in fall 2013. The combined cryostat, cryogenic and storage system (ReStoX) were successfully commissioned in summer of 2015. In November 2015 the TPC was attached to the inner cryostat inside the water shield. Afterwards, the commissioning work started, followed by the detector characterisation and calibration campaign. The detector was filled with 3.2 t of liquid xenon from ReStoX in mid-April 2016. The operation lasted about two weeks, reaching a filling speed of 650 kg/day after the initial cool-down period. The core xenon handling systems performance met or exceeded the design specifications and the filling operation was completed. With the cryostat filled, the cryogenic system has been in continuous operation for the last months, maintaining the liquid xenon at constant temperature and pressure (temperature rms $<$0.04 C, pressure rms $\sim$ 1 mbar). The first science run started in November 2016. The TPC is thus filled with liquid xenon since April 2016, and the primary scintillation (S1) as well as the delayed proportional signal from the charge (S2) are recorded by the two arrays of 248 PMTs, where 127 are placed above, and 121 below the LXe target. For each interaction, the PMTs observe a certain number of photoelectrons (pe). For the initial science run, the drift field is similar to the one in LUX (0.16 kV/cm), after which the field will be increased. The electron extraction field is around 10 kV/cm, and ensures 100% electron extraction efficiency. The electron lifetime is around 600 µs, and linearly increasing due to the online purification of the liquid. Figure 4.3, shows the science data acquisition period, interspersed by various calibration runs with external and internal sources. Due to several earthquakes on January 18, after which the detector required a few days to recover (trip of the TPC high voltages, LXe level oscillations), we decided to analyse the first $\sim$34 live days and release initial results in early sum-

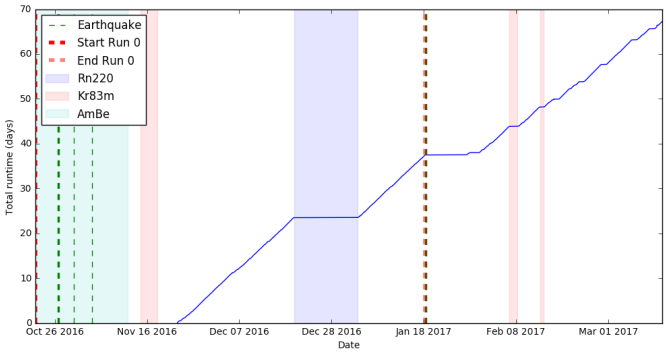

FIG. 4.3 – The science data taking period (runtime in days, shown as blue curve), interspersed by calibration runs with external and internal sources such as AmBe (NR band), ^{83m}Kr (energy scale) and ^{220}Rn (ER band).

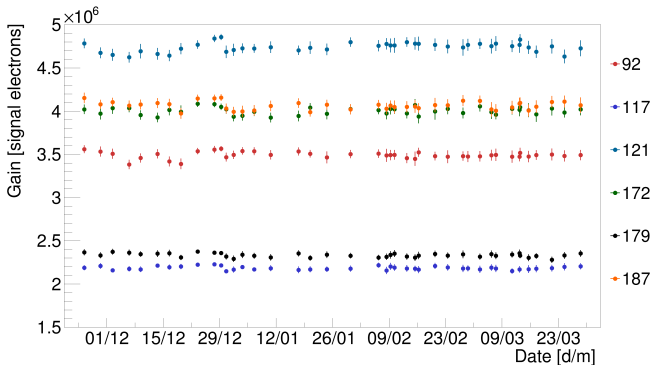

FIG. 4.4 – An example of the gain evolution during several months for 6 PMTs in XENON1T.

mer 2017. A combination of this data with the new science data (>45 days as of now) will follow.

We are responsible for the in-situ calibration of the photomultiplier tubes and monitor their stability in time, including the after-pulse rates. Three independent gain measurement methods were developed in our group and implemented for the routine calibration of the PMTs. These are based on external LEDs and low-intensity (single photon) scintillation pulses from particle interactions, and yield consistent results within the systematic uncertainties of each method. An example of long-term stability for 6 PMTs is shown in Fig. 4.4. We have developed a database (DB) based on an open-source MySQL management system, to store and monitor various operational parameters of the PMTs, such as gain, single photoelectron resolution, after-pulse and dark count rates, and track their long-term stability. Other information, e.g. radioactivity values and laboratory tests for each phototube, is also stored in the same DB, allowing us to study correlations between various parameters.

We substantially contribute to the analysis of the calibration and science data of the XENON1T experiment, from the development and validation of the data quality selection criteria to the final physics analyses. We contributed to the first XENON1T science run (end Nov 2016 - January 18, 2017) with algorithms for event selection, event vertex reconstruction, signal corrections and energy calibrations. We are continuing our work on data from this run, as well as from the second run (that started in February 2017) and will focus on various physics analyses of the first science as well.

4.3 The XENONnT and DARWIN project

In parallel to the ongoing XENON1T analysis work, we are working on a new TPC design for the planned upgrade, XENONnT. Many of the major components in XENON1T are constructed such that an upgrade to a detector housing more than twice the amount of LXe will become feasible once the science goals of XENON1T are achieved. However it requires the construction of a new inner cryostat and a new TPC. We are co-responsible for the design, fabrication, assembly, and testing of the new TPC. The design will be largely based on the configuration which we have developed for XENON1T, with confirmed stability in liquid xenon as well as sufficiently low radioactivity levels but with a 40% increase in linear dimensions. The increased size of the TPC, accommodating a liquid-xenon total (active target) mass of 7.5 t (6.0 t), will improve the sensitivity by a factor of ten.

As polytetrafluorethylen (PTFE) efficiently reflects the scintillation light from liquid xenon, the internal surfaces of the field cage will consist of interlocking side panels of polished PTFE and self-centring PTFE disks to surround the PMTs on the top and bottom of the field cage. This design accommodates for PTFE shrinkage at cryogenic temperatures. Because the fluorine in PTFE has a very high cross section for (α,n) reactions, an effort was made to replace the PTFE in areas where it is not essential. Therefore the support structures will be made of Torlon, for it has good structural properties, a high dielectric constant, and a much lower expected contribution to the neutron background. The first samples for the main XENONnT TPC materials have been procured and their screening is underway.

We are responsible for the production of the voltage-divider circuits for the XENONnT PMTs, which will provide good linearity in the full DAQ range while maintaining high single-photon sensitivity at a gain of 2×10^6, with a power distribution below 0.25 W/channel. The design will be largely based on the configuration which we have developed for XENON1T. We initiated a study of the outgassing properties of various substrates (e.g. Cirlex and CuFlon) for the printed circuits with a dedicated facility at UZH [20], and the design will be optimised based on the obtained results, together with the information from the radioactive screening campaign with γ- and mass-spectrometry.

We have to guarantee that all of the XENONnT PMTs will not fail during the lifetime of the XENONnT detector. For this purpose the PMT testing facility for the XENON1T PMTs at UZH has been upgraded. The upgrade, shown in Fig. 4.5, can house 10 PMTs simultaneously, allowing for more efficient PMT qualification measurements.

To amplify the PMT signals induced by low-energy interactions in the target, and thus improve the single photon detection efficiency, in XENON1T we use commercial linear amplifiers (Phillips 776). Since XENONnT and DARWIN will start to have a competitive sensitivity to the neutrinoless double-beta decay [21,22], where the energy region of interest is around 2.5 MeV, we are working on the design and optimisation of an amplifier circuit to increase the dynamic range. Several prototypes have been developed and characterised, and the current configuration is based on an asymmetrically polarised operational amplifier LMH6629, and an additional wide-band, low-distortion OPA842 from Texas Instruments. It features a low input voltage noise of 0.69 nV/$\sqrt{\text{Hz}}$, input current noise of 2.6 pA/$\sqrt{\text{Hz}}$, and a high bandwidth of

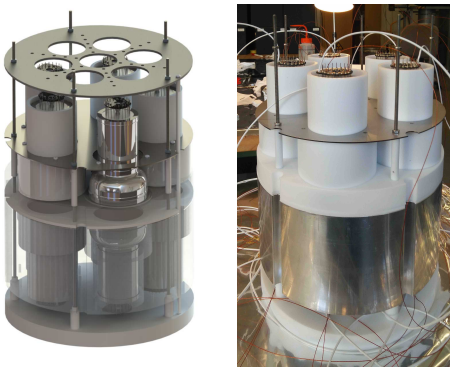

FIG. 4.5 – The inner part of the MarmotXL photosensor test facility at the UZH (drawing, left and a picture, right). The aluminium filler reduces the amount of xenon required to cover the phototubes, while the PTFE jackets insulate the metal bodies. A larger cryostat vessel, not shown here, provides the vacuum insulation during cryogenic operation. The previous version of the facility is also described in [23].

900 MHz. The output signal is split into two channels, hence one is attenuated by a factor of two, while the other is amplified by a factor of ten. A 8-channel NIM board is under construction and will be tested in-situ with the XENON1T data acquisition system.

[20] Walter, M., Ph.D. Thesis, University of Zurich, 2015.

[21] E. Aprile *et al.* [XENON Collaboration], JCAP **1604** (2016) no.04, 027.

[22] L. Baudis, A. Ferella, A. Kish, A. Manalaysay, T. Marrodan Undagoitia and M. Schumann, JCAP **1401** (2014) 044.

[23] P. Barrow *et al.*, JINST **12** (2017) no.01, P01024.

4.4 R&D for XENON and DARWIN

The Xurich II detector has been designed to measure the scintillation and ionisation yields of LXe from low-energy nuclear recoils. The measured volume-averaged light yield at 9.4 keV is 15.0 pe/keV at zero field, and 10.8 pe/keV at a drift and extraction field of $\sim$1 kV/cm and $\sim$10 kV/cm, respectively. Together with a high yield S2 signal of $\approx 2\times10^3$ pe/keV, this allows us to reach a sub-keV energy threshold. The energy resolution from the combined S1 and S2 signals is (5.8$\pm$0.3)% at 32 keV, comparable to state-of-the-art $xy-$position sensitive LXe detectors [24].

The z-coordinate of an interaction in a dual-phase TPC is linearly related to the measured delay time between the S1 and S2 signals. This dependence, together with the precise knowledge of the physical dimension of the TPC, allowed us to measure the drift velocity of electrons (at 184 K) for electric fields from $\sim$0.2 to $\sim$1.3 kV/cm, relevant for current and future large-scale dual-phase xenon TPCs. As shown in Fig. 4.6, the measured electron drift velocity ranges from

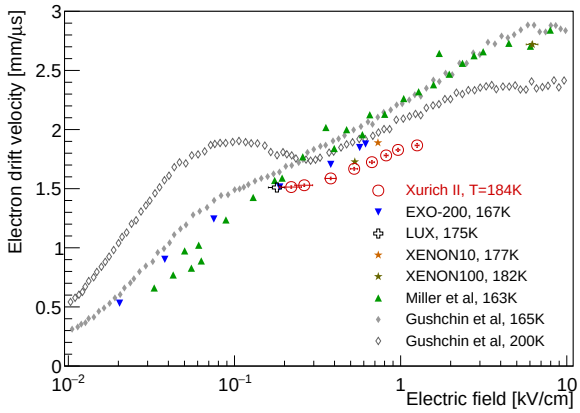

FIG. 4.6 – Electron drift velocity as a function of electric field measured with Xurich II (open red circles), together with literature values [25–30].

1.63 to 2.00 mm/µs, and we observe good agreement with other measurements performed at similar temperatures. A manuscript detailing these results, along with the description of the detector and its commissioning data, is under preparation. The detector is currently acquiring data at the D-D fusion neutron generator facility at UZH. We use Compton scatters of 662 keV γ-rays from a ^{137}Cs source to characterise the TPC response to electromagnetic interactions, and elastic neutron scatters at all angles to study the nuclear recoils at low energies.

To calibrate the Xurich II detector down to energies of $\sim$1 keV, we are developing a method for the injection of ^{37}Ar gas into the active volume of the detector. This isotope can be produced by neutron irradiation of natural argon gas at the neutron activation station of the SINQ facility at the Paul Scherrer Institute, similar to the method in [31]. The ^{37}Ar decay will provides two low-energy lines, at 2.82 keV and 0.27 keV, following the K- and L-shell electron capture. Such a calibration will not only provide relevant information for our study of low-energy xenon response with Xurich II, but will also be used to develop a new low-energy calibration standard for large-scale detectors such as XENON and DARWIN.

[24] S. Stephenson *et al.*, JINST **10** (2015) no.10, P10040.

[25] E. Aprile *et al.* [XENON Collaboration], Astropart. Phys. **54** (2014) 11.

[26] E. Aprile *et al.* [XENON Collaboration], J. Phys. G **41** (2014) 035201.

[27] L. S. Miller, S. Howe and W. E. Spear, Phys. Rev. **166** (1968) 871.

[28] P. F. Sorensen, Ph.D. Thesis, Brown University, 2008.

[29] D. S. Akerib *et al.* [LUX Collaboration], Phys. Rev. Lett. **112** (2014) 091303.

[30] J. B. Albert *et al.*, Phys. Rev. C **95** (2017) no.2, 025502.

[31] S. Sangiorgio *et al.* [EXO-200 Collaboration], Nucl. Instrum. Meth. A **728** (2013) 69.

5 Searching for Dark Matter and Neutrinos with CCD Detectors

J. Liao, B. Kilminster, and P. Robmann

in collaboration with: Fermi National Accelerator Laboratory, University of Chicago, University of Michigan, Universidad Nacional Autónoma de México, Universidad Nacional de Asunción de Paraguay

(DAMIC Collaboration)

Using thick, fully-depleted, low-noise CCDs, we are able to search for low-energy nuclear recoils which produce a small number of ionization electrons. The DAMIC (Dark Matter in CCDs) experiment uses this technology to provide high sensitivity for directly detecting weakly interacting dark matter (DM) particles (WIMPs) with mass below 5 GeV. The CONNIE (Coherent Neutrino Nucleus Interaction) experiment uses the same type of detector to search for the process of neutrinos scattering coherently off nuclei, a process which is predicted by the standard model, but has currently never been experimentally observed.

5.1 DAMIC

DAMIC searches for low-mass DM which is motivated by the similar abundances of baryons and DM, and the disparity of the matter-antimatter densities [1–3]. First results for DAMIC were obtained from data collected in 2011 [4]. At that time, these DAMIC results constituted the best limits for DM mass below 4 GeV, but have been superseded since. The main challenge in searching for low mass DM is measuring the low energy deposit of the associated nuclear recoils in the detection material. DAMIC uses CCDs with an electronics noise of σ=7.2 eV corresponding to a 5σ=36 eV threshold, which is the lowest of any current DM detector. CCD detectors are silicon pixel detectors that shift charge from the capacitor of one pixel to the next by generating potential wells until reaching a charge amplifier which converts the charge to voltage (Fig. 5.1). The DAMIC CCD detectors were fabricated by Lawrence Berkeley National Laboratory [5] originally for the Dark Energy Camera (DECam) [6, 7]. DECam CCDs [8] are 30 times thicker (500 - 650 µm) than commercial CCDs, leading to correspondingly higher detection efficiencies. Each CCD has up to 16 million 15 µm x 15 µm pixels and is read out by two amplifiers in parallel. The electronic gain is $\sim$ 2.5 µV/e. The signal is digitized after correlated double sampling and the noise performance improves by reducing the readout speed. The lowest noise, $\sigma < 2e^-$ (R.M.S.) per pixel, was achieved with readout times of 50 µs per pixel [9].

In 2015, the upgraded DAMIC experiment collected data in SNOLab, which boasts 6000 meter-water-equivalent of overburden that provides shielding from backgrounds induced by cosmic ray muons. This new DAMIC experiment took 0.6 kg·days of data using four 5.5-gram CCDs, each 5 times the mass of those used in the previous experiment. The CCDs are installed inside a copper box cooled to -150°C to reduce dark current. The cold copper also shields the detectors against infrared radiation. A closed cycle helium gas refrigerator is used to maintain the low temperature. Lead and polyethylene shield against γ-rays and neutrons. The detector is connected through a readout cable to the preamplifiers located outside the lead shield. The detector package is housed in a cylindrical vacuum vessel fabricated with oxygen-free copper, and maintained at 10^{-7} Torr with a turbo molecular pump. Results of this data run were published in 2016 [10], showing that DAMIC is competitive with other low-mass DM searches.

Given the low energy threshold and excellent energy resolution to resolve low energy signals, DAMIC has discovered a niche for searching for different types of DM candidates. One such candidate is known as the hidden photon [11]. Like an ordinary photon, a hidden photon can be absorbed by an electron in a detector material. However, the hidden photon would have a mass and be non-relativistic, allowing it to clump in DM halos in the manner of weakly interacting massive particles. One interesting difference of hidden photons with respect to

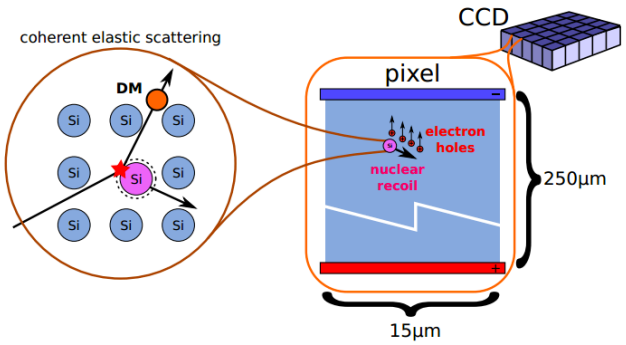

FIG. 5.1 – DAMIC detection principle: hypothetical DM particles scatter coherently off silicon nuclei, producing a nuclear recoil that is recorded as charge on pixels in the CCD. A prototype setup with a CCD thickness of 250 µm is shown.